

# Subsurface warming derived by Argo floats during the 2022

## Mediterranean marine heatwave

Annunziata Pirro<sup>1</sup>, Riccardo Martellucci<sup>1</sup>, Antonella Gallo<sup>1</sup>, Elisabeth Kubin<sup>1</sup>, Elena Mauri<sup>1</sup>, Mélanie Juza<sup>2</sup>, Giulio Notarstefano<sup>1</sup>, Massimo Pacciaroni<sup>1</sup>, Antonio Bussani<sup>1</sup>, Milena Menna<sup>1</sup>

<sup>1</sup>National Institute of Oceanography and Applied Geophysics (OGS), Trieste, 34010, Italy

<sup>2</sup>Laboratory Balearic Islands Coastal Observing and Forecasting System (SOCIB), Palma, 07122, Spain

*Correspondence to:* Annunziata Pirro (apirro@ogs.it)

### **Abstract.**

The Mediterranean marine heatwave (MHW) during the warm season (May-September) and the fall period (October-December) of 2022 is analyzed using Argo float in-situ observations in the upper 2000 m of depth. Five study regions (North Western Mediterranean, South Western Mediterranean, central Ionian Sea, Pelops Gyre and south Adriatic Pit) most affected by warming in different layers were selected and investigated. Temperature anomaly profiles  $T_a(z)$  computed for each area and for both periods were divided into three categories based on vertical heat penetration: Category 1 (shallow, 0-150 m), Category 2 (intermediate, 150-700 m) and Category 3 (deep, > 700 m). During the warm season, Category 1 profiles had a temperature anomaly near zero or slightly negative in a thin layer between 50 m and 150 m depth, while warming was observed in the 0-50 m layer and below the middle layer. Profiles characterized by greater vertical heat penetration (categories 2 and 3) were mainly in mesoscale or sub basin structures and showed the largest positive temperature anomaly in the surface and intermediate layers. All profile categories showed a warming between 200 and 800 m depth. This increase is roughly split, with half attributed to the impact of the 2022 MHW, and the other half linked to the ongoing long-term trend in ocean temperatures. During the fall period and in the layer below 200 m depth, the shape of the  $T_a$  profiles are similar for all sectors with the exception of the south Adriatic Pit, which depict a  $+0.5^\circ\text{C}$  warming at 800 m depth.

The present work highlights the warming characteristics along the entire water column in different regions of the Mediterranean Sea, some of which are characterized by dynamic activities (e.g. dense water formation, upwelling) therefore, any variation of the associated ocean processes can have implication on the thermohaline circulation and thus, on the climate system.

## 28 Introduction

29 Marine heatwaves (MHWs) are extreme ocean temperature events occurring over extended periods of time (Hobday et al.,  
30 2016). Over the past decade the frequency of MHW events has increased by 50% (IPCC, 2023) as well as their duration and  
31 magnitude (Oliver et al., 2018). They can affect small areas of coastline or span multiple ocean areas across latitudes with  
32 significant impacts on ecosystems, coastal communities and economies (Wernberg et al., 2013; Garrabou et al., 2022; Dayan  
33 et al., 2023).

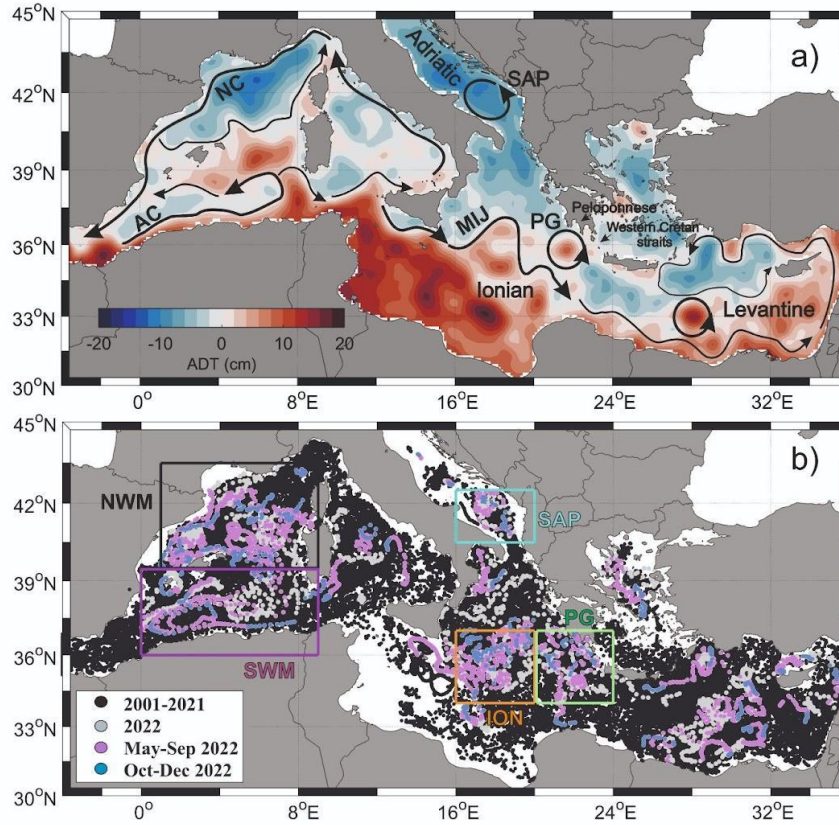
34 Since the beginning of the 21<sup>st</sup> century the particularly rapid warming trend of the Mediterranean Sea surface layer has been  
35 associated with a strong increase in MHWs events (Bensoussan et al., 2019, Ibrahim et al, 2021, Juza et al., 2022, Pastor and  
36 Khodayar, 2022, Dayan et al., 2023). Several studies, mainly confined at the surface, have addressed this topic covering  
37 different aspects of MHWs using satellite observations and model simulations. In particular, from basin to sub-regional scale,  
38 previous works analyze MHWs drivers and indicators, estimate the frequency, the duration and intensity of MHWs, evaluate  
39 their trend and assess the risk and the impacts on ecosystems (Darmaraki et al 2019, Galli et al., 2017, Garrabou et al., 2022,  
40 Juza et al., 2022, Dayan et al., 2023, Martinez et al., 2023, Marullo et al., 2023, Pastor and Khodayar, Simon et al., 2023).  
41 However, MHWs are not exclusively limited to the surface layer, but they can also propagate throughout the deeper layers of  
42 the water column (Darmaraki et al., 2019, Shijian et al., 2021, Scannell H.A., 2020, Juza et al., 2022). This can cause negative  
43 ecological consequences compromising the maintenance of the biodiversity, of the food and the regulation of air quality  
44 (Garrabou et al., 2022; Holbrook et al., 2020; Santora et al., 2020; Smale et al., 2019; Schaeffer and Roughan, 2017; Lique  
45 et al., 2016; Martín-Lopez et al., 2016; Mills et al., 2013). A recent work in the Mediterranean Sea shows that although MHWs  
46 frequency is higher at the surface, their maximum intensity and duration is registered in the subsurface layers (Dayan et al.,  
47 2023). Moreover, in-situ data collected in the tropical western Pacific Ocean show that the maximum intensity of almost every  
48 MHW event is found in the subsurface layer, and many of the MHWs occurred even when no significant warming anomalies  
49 are detected at the surface (Shijian et al., 2021). **Using satellite data, Marullo et al. (2023) defined the occurrence of the event  
50 in the Mediterranean Sea from May 2022 to spring 2023, with higher intensity in summer 2022 and in the band 0°-25° E.**  
51 Starting from this result, the present work analyzes the subsurface properties of the 2022 MHW in the upper 2000 m depth  
52 using in-situ hydrographic Argo profiles (Product ref. no. 1, Table 1; Wong et al., 2020) collected during the period of highest  
53 intensity (warm season, May-September) and in the period thereafter (cold season, October-December). Focusing on Marullo  
54 et al. (2023) results and on the availability of Argo float profiles, five study areas were selected for our analysis (Figure 1(b)).  
55

56

57

58

Product ref. no.	Product ID & type	Data access	Documentation
1	INSITU_MED_PHYBGCWAV_DISCRETE_MYNRT_013_035; In-situ observations	EU Copernicus Marine Service Product, 2022a;	Quality Information Document (QUID): Wehde et al., (2022) Product User Manual (PUM): In Situ TAC partners (2022)
2	MEDSEA_MULTIYEAR_PHY_006_004; numerical models	EU Copernicus Marine Service Product, 2022b;	Quality Information Document (QUID): Escudier al., (2022) Product User Manual (PUM): Lecci et al., (2022)
3	SEALEVEL_EUR_PHY_L4_NRT_OBSERVATIONS_008_060; satellite observations	EU Copernicus Marine Service Product, 2023;	Quality Information Document (QUID): Pujol al., (2023) Product User Manual (PUM): Pujol., (2022a)
4	SEADATANET_MedSea_climatology_V2; climatology	SEADATANET Product; 2022	Product Information Document (PIDoc): Simoncelli et al. (2020)



62 **Figure1: (a) Absolute Dynamic Topography (colours) averaged from spring-summer (May-September 2022) along with schematic**  
 63 **pathways (black arrows) of the Algerian Current (AC), Northern Current (NC), Mid-Ionian Jet (MIJ), South Adriatic Pit (SAP)**  
 64 **and Pelops Gyre (PG). (b) Argo floats position for the whole Mediterranean Sea. Black, magenta, cyan, orange and green boxes**  
 65 **indicate the North West Mediterranean (NWM, 39.5-43.5°N; 1-9°E), South West Mediterranean (SWM, 36-39.5°N; 0-9°E), South**  
 66 **Adriatic Pit (SAP, 40.5-42.5°N; 16-20°E), Ionian (ION, 34-37°N; 13-20°E) and Pelops Gyre (PG, 34-37°N; 20-24°E) areas,**  
 67 **respectively. (c-e) 2022 Ocean Heat Content (OHC) anomaly estimated every meter with respect to the 2001-2018 FLOAT**  
 68 **climatology period from Argo floats profiles in different layers (c, 5-150m), (d, 150-700), (e, 700-2000).**

69 Based on the vertical heat penetration (MHW depth, see Methods section), the temperature profiles collected in May-  
70 September 2022 from each study area were divided into three categories (shallow, intermediate and deep penetration) and the  
71 median profile of temperature anomaly ( $\tilde{T}_a$ ) was computed for each of them. Changes in the vertical temperature anomalies  
72 were described and analyzed in relation to the ocean stratification, circulation and dynamics of each specific area. Lastly, this  
73 study examines the properties of the water column during the fall period and speculates on its relationship with the dynamics  
74 of the previous warm season's MHW. An estimation of the horizontal and vertical distribution of the Ocean Heat Content  
75 (OHC) anomaly in 2022 was also performed in the whole Mediterranean Sea (Figures 1c-e).

76

## 77 **Methods**

78 The vertical propagation of the 2022 MHW in the Mediterranean Sea was investigated using temperature data collected by  
79 Argo floats in the period 2001-2022 (Figure 1(b)). These data were collected and made freely available by the International  
80 Argo Program (which is part of the Global Ocean Observing System (Argo 2023)) and by the national program Argo Italy that  
81 contributes to it (<https://argo.ucsd.edu>, last access 23 April 2023; <https://www.ocean-ops.org>, last access 23 April 2023).

82 A comprehensive characterization of the event over the whole Mediterranean Sea was performed starting from the OHC  
83 analysis. The OHC, defined as the total amount of heat absorbed and stored by the ocean, can be considered as a good indicator  
84 for assessing the Earth's energy imbalance (Von Schuckmann et al., 2016). A float derived OHC climatology (OHC<sub>2001-2018</sub>)  
85 for the period 2001-2018 was estimated in 1° x 1° bins and in different layers (0-150 m, 150-700 m, 700-2000 m) using the  
86 method of Kubin et al., 2023. Subsequently, Argo temperature data collected in 2022 were averaged on the same grid of  
87 OHC<sub>2001-2018</sub> to compute the 2022 OHC (OHC<sub>2022</sub>). The OHCA<sub>2022</sub> was then calculated as the difference between OHC<sub>2022</sub> and  
88 OHC<sub>2001-2018</sub> fields.

89 The five Mediterranean Sea regions most affected by surface warming (Figure 1b) were selected using the results of Marullo  
90 et al. (2023) and considering the availability of float data. In these regions we analyzed the vertical penetration of the 2022  
91 MHW signal in the water column both during the warm and cold season. The regions selected are: the North Western  
92 Mediterranean (NWM), the South Western Mediterranean (SWM), the Ionian (ION), the Southern Adriatic Pit (SAP) and the  
93 Pelops Gyre (PG) sectors.

94 The Temperature anomaly  $T_a$  at each depth  $z$  and for each profile was computed as:

$$T_a(z) = T(z) - \bar{T}(z), \quad (1)$$

95 for each sector.  $T(z)$  is the 2022 temperature derived from Argo floats while  $\bar{T}(z)$  is the climatological (1985-2018) averaged  
96 temperature derived from the SeaDataCloud dataset (Product ref. no. 4, Table 1; SDC climatology). Specifically, the gridded

97 (0.125° x 0.125°) monthly climatological profiles were linearly interpolated in depth (every 10 m) and at the position of each  
 98 float profile. Moreover, to compare the 2022 MHW event with the averaged conditions estimated by floats in the selected  
 99 sectors,  $T_a$  profiles were also computed for the whole float dataset in the period 2001-2018 (FLOAT climatology). **It's important**  
 100 **to highlight that while this study utilizes the SDC climatology, the FLOAT climatology was utilized to facilitate a**  
 101 **straightforward comparison with the OHC findings from Kubin et al. (2023).** The time window used for the present work  
 102 (May-September 2022) was chosen based on the latest European Space Agency specification  
 103 ([https://www.esa.int/Applications/Observing\\_the\\_Earth/Mediterranean\\_Sea\\_hit\\_by\\_marine\\_heatwave](https://www.esa.int/Applications/Observing_the_Earth/Mediterranean_Sea_hit_by_marine_heatwave), last access 18  
 104 February 2023) and on the estimations of Marullo et al. (2023). These indicate that the 2022 MHW developed in the second  
 105 half of April in the northwest Mediterranean Sea and extended over the central Mediterranean into September. In this period,  
 106  $T_a$  profiles were quality controlled to remove any inconsistency (e.g. profiles with negative surface anomalies) and used to  
 107 estimate the vertical propagation of the MHW (or MHW depth), following the method of Elzahaby and Schaeffer 2019. For  
 108 each profile, the positive threshold depth (hereafter  $Z_N$ ) is defined as the depth at which the first negative or 0 temperature  
 109 anomaly occurred:

$$Z_N = \min (z(T_a(z) \leq 0)), \quad (2)$$

110 Knowing  $Z_N$ , the vertical cumulative temperature anomaly ( $CT_a$ ) defined as:

$$CT_a(Z_N) = \sum_{z=0}^{Z_N} T_a(z) \Delta z, \quad (3)$$

111 with  $\Delta z = 10$  m, was computed for each profile from the surface ( $z=0$ ) to the positive threshold depth ( $z=Z_N$ ). To reduce the  
 112 effect of the insignificant warming at depths per water profile, we define the MHW depth as the depth where a fraction ( $\varepsilon=0.95$ )  
 113 of the cumulative  $T_a$  is reached:

$$MHWdepth = \max (z(CT_a(z) \leq \varepsilon \cdot CT_a(Z_N))), \quad (4)$$

114 Based on MHW depth values,  $T_a$  profiles were then divided into three categories: Category 1 (shallow, 0-150 m), Category 2  
 115 (intermediate, 150-700 m) and Category 3 (deep, > 700 m). It's noteworthy that within the SAP area, float profiles categorized  
 116 as Category 2 and Category 3 consistently exhibit no negative temperature anomalies. However, they are classified into these  
 117 categories based on their respective depths, shallower or deeper than 700 meters. Additionally, despite the limited number of  
 118 profiles available in this region, they all fall within the cyclonic gyre. Hence, we are confident in considering them as  
 119 representative of the entire SAP region. The median profile ( $\tilde{T}_a$ ) for each category was obtained by spatially averaging all the  
 120 available data in the different sectors in the warm period using 2022 and FLOAT climatology Argo data. Considering that the  
 121 2022 MHW extends until the spring of 2023, (Marullo et al., 2023), the median profiles  $\tilde{T}_a$  for the fall period were also  
 122 examined to investigate the accumulation of the heat in the water column. The mean  $T_a$  averaged in the surface, intermediate

123 and deep layers as well as other additional information (number of profiles, MHW depth, max  $T_a$  and depth of max) are listed  
124 in Table 2.

125 Lastly, the Brunt-Väisälä frequency squared ( $N^2$ ) for the year 2022 and in the upper 150 m depth was computed using monthly  
126 averaged temperature and salinity Argo floats profiles for each sector in order to support the vertical heat penetration. The  
127 same procedure was adopted to calculate the  $N^2$  anomaly with respect to FLOAT climatology.

128

129

130

131

132

133

134

135

136

137

138

139

140

141

142

143

144

145

146

			Number of observations	MHW depth (m)	Temperature anomaly			averaged values		
					Surface (10 m)	Max	Depth of max (m)	0-150 m	150-700 m	700-2000 m
<b>NWM</b>	spring summer	C1	335	24,8	2,3	5,82	22,5	*0,28	0,32	0,097
		C2	16	571,9	2,2	5,48	50	0,32	0,4	NaN
		C3	43	1457,9	2,92	5,58	19,5	0,8	0,36	0,1
		clim	-	-	-	-	-	0,12	0,06	0,025
	fall	fall	306	-	-	-	-	0,66	0,33	0,11
		clim fall	-	-	-	-	-	0,08	0,07	0,04
<b>SWM</b>	spring summer	C1	159	25,6	2,13	5,79	22,5	0,19	0,33	0,088
		C2	5	630	1,83	5,46	24	0,43	0,3	NaN
		C3	27	1409,6	2,24	5,05	24,1	0,86	0,36	0,095
		clim	-	-	-	-	-	0,028	0,059	0,028
	fall	fall	148	-	-	-	-	0,18	0,31	0,11
		clim fall	-	-	-	-	-	0,1	0,05	0,02
<b>ION</b>	spring summer	C1	105	22,8	1,34	4,58	22,2	0,03	0,27	0,12
		C2	5	644	2,18	2,87	18	0,58	0,35	0,54
		C3	3	1383,4	1,39	1,97	20	0,47	0,54	0,15
		clim	-	-	-	-	-	0,071	0,091	0,057
	fall	fall	119	-	-	-	-	-0,21	0,26	0,12
		clim fall	-	-	-	-	-	-0,06	0,07	0,05
<b>PG</b>	spring summer	C1	50	37	1,34	3,82	41	0,15	0,32	0,03
		C2	15	553,4	0,95	6,15	47,3	0,97	0,34	0
		C3	20	1043,5	0,88	5,34	40	1,14	0,58	0,05
		clim	-	-	-	-	-	0,3	0,15	0,02
	fall	fall	70	-	-	-	-	-0,2	0,19	-0,02
		clim fall	-	-	-	-	-	0,27	0,13	0
<b>SAP</b>	spring summer	C1	9	32,2	1,18	3	24,5	0,57	0,39	0,66
		C2	10	411	1,95	7,25	27	1,04	0,46	NaN
		C3	17	945,3	0,88	4,36	78,8	0,72	0,4	0,59
		clim	-	-	-	-	-	0,3	0,21	0,21
	fall	fall	44	-	-	-	-	0,27	0,41	0,69
		clim fall	-	-	-	-	-	0,29	0,2	0,16

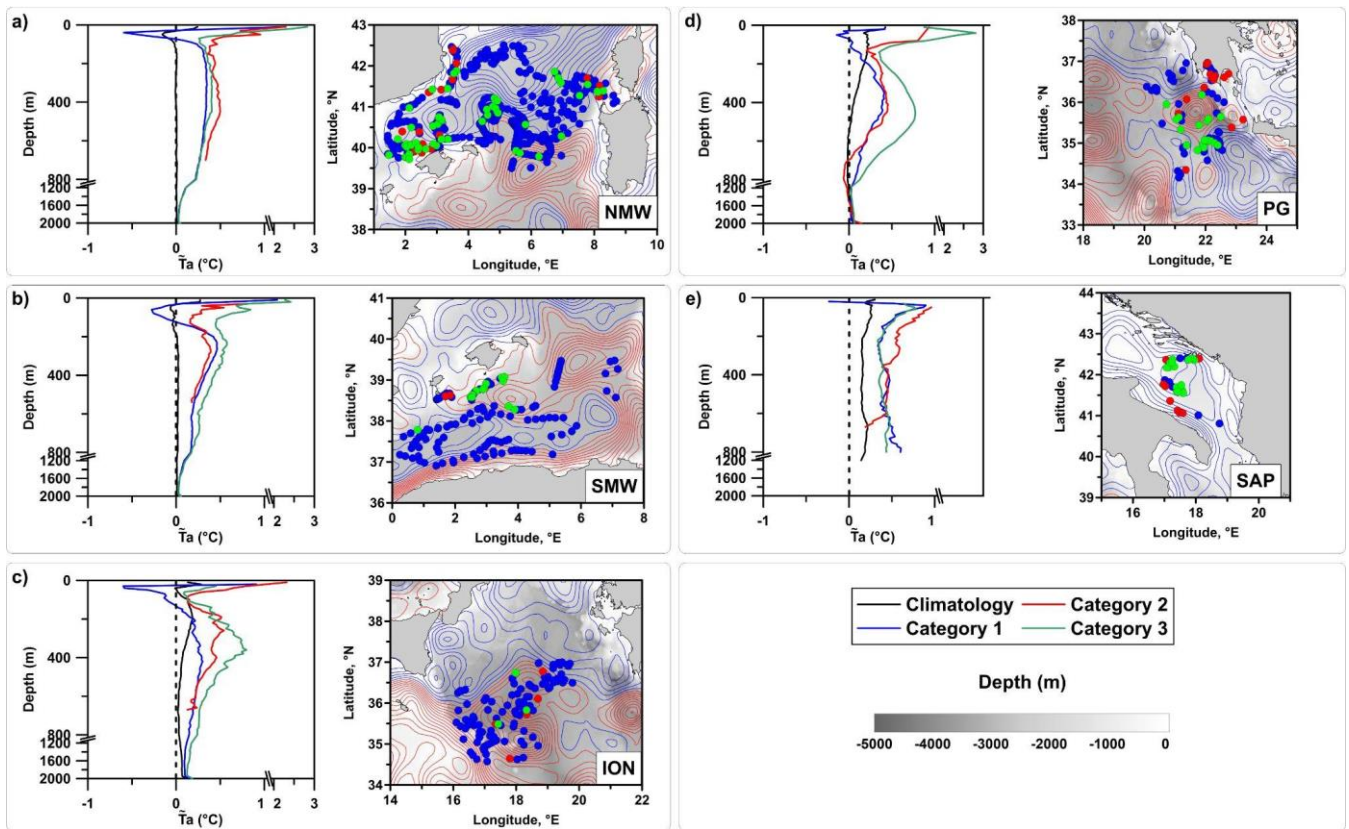


148 **Table 2: Characteristics of the 2022 MHW in Category 1(C1), Category 2 (C2), Category 3 (C3): MHW depth, surface temperature**  
149 **anomaly (Surface), maximum temperature anomaly (Max) and the depth where it occurs (Depth of max), mean temperature**  
150 **anomaly for the surface (0-150 m), intermediate (150-700 m) and deep (700-2000 m) layers for each category and for the FLOAT**  
151 **Climatology (clim).**

152

## 153 **Results and discussion**

154 In the surface layer, the  $\text{OHCA}_{2022}$  displayed inhomogeneous warming patterns, with positive anomalies areas adjacent to  
155 others with strong negative anomalies (Figure 1(c)). Largest positive anomalies were observed in the West Mediterranean, in  
156 the South Adriatic, in the eastern Ionian and northern Levantine basin. In the intermediate and deep layers the warming was  
157 more homogeneous and widespread (Figures 1(d), 1(e)) where the majority of bins showed positive values of the  $\text{OHCA}_{2022}$   
158 and specifically, the western and central Mediterranean areas along with the Aegean Sea showed a more pronounced warming  
159 compared to the Levantine basin, which exhibits a slight cooling in some bins of the central and eastern sectors. It can be stated  
160 that half of this warming in the intermediate and deep layers is due to the 2022 MHW while the other half to the long-term  
161 warming of the ocean. This consideration stems from comparing the current  $\text{OHCA}_{2022}$  with OHC trends defined by Kubin et  
162 al. (2023). To perform this study, five regions (NWM, SWM, ION, SAP and PG; coloured boxes in Figure 1(b)) were selected.  
163 This choice was motivated by the highest 2022 SST anomaly registered in the band 0 - 25° E (Marullo et al. 2023) and by the  
164 availability of float data in both May-September and October-December 2022 periods. Figure 2 shows  $\tilde{T}_a$  profiles for the warm  
165 season of each sector, for each MHW depth category and for the FLOAT climatology.



166

167 **Figure 2: (left panels) Median profiles of temperature anomaly computed for each sector (NWM, SWM, ION, PG, SAP) and for the**  
 168 **2022 warm season (May-September) using Argo floats data with respect to the 1985-2018 SDC climatology dataset. Black lines**  
 169 **highlight the FLOAT climatology profiles while blue, red and green profiles indicate shallow (0-150 m), intermediate (150-700 m)**  
 170 **and deep (> 700m) categories, respectively. (right panels) Positive and negative contours of the Absolute Dynamic Topography with**  
 171 **1 cm spacing are displayed by red and blue lines while the coloured dots are associated to the floats position of each category.**

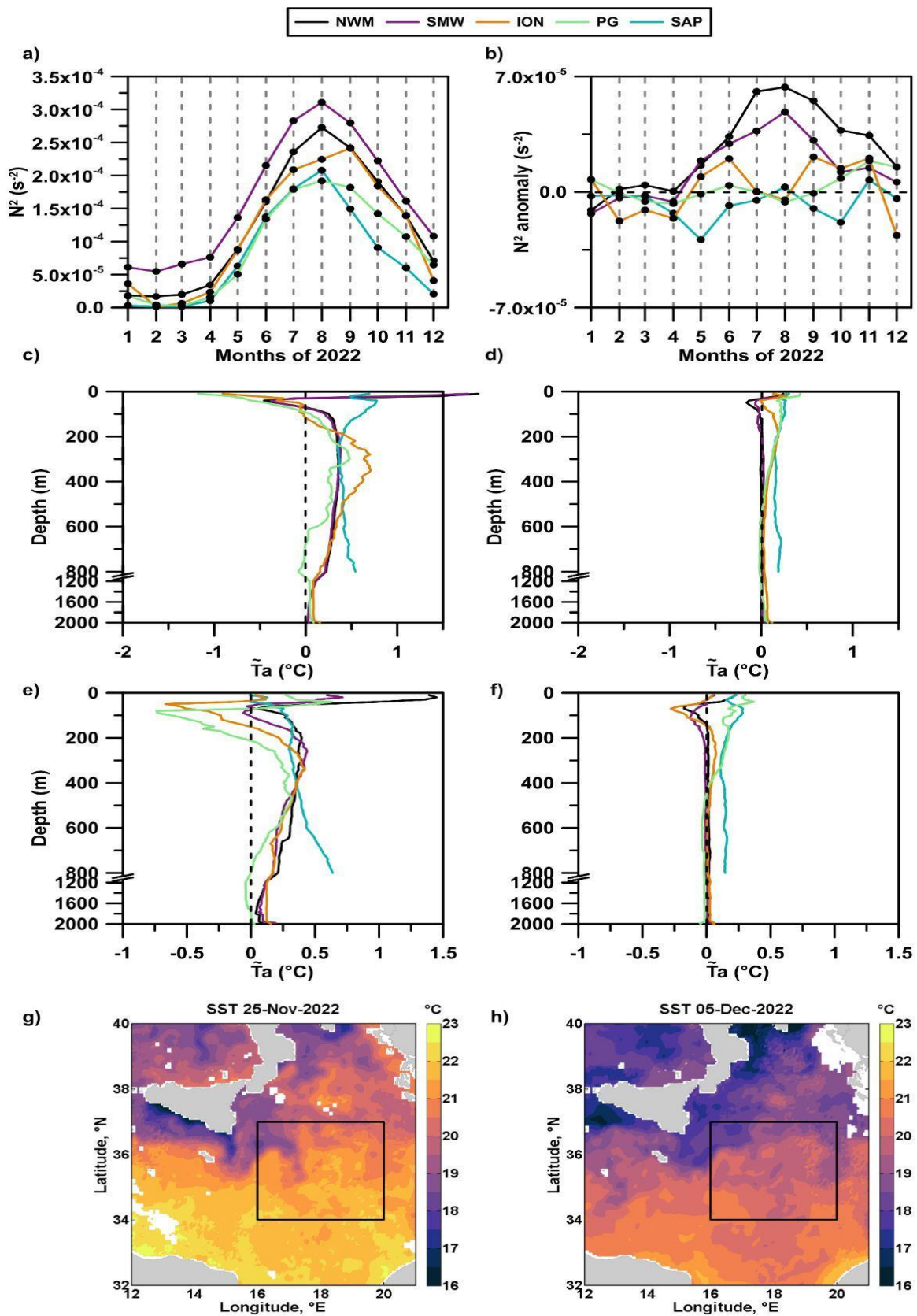
172 In the NWM and SWM sectors the circulation is strongly influenced by the presence of two intense and permanent currents  
 173 (Figure 1(a)): the south-westward Northern Current (Poulain et al., 2012; Escudier et al., 2021) and the eastward along-slope  
 174 Algerian Current (which transports waters of Atlantic origin in the upper water column (Poulain et al., 2021)) in the NWM  
 175 and in the SWM, respectively. Therefore, float profiles were mainly located along the boundary of cyclonic circuits as  
 176 highlighted by the Absolute Dynamic Topography (Product ref. no. 3, Table 1; (Figures 2(a), 2(b)). In the ION sector, float  
 177 profiles were mainly distributed in the anticyclonic meander of the Mid-Ionian Jet (Figure 2(c)), a strong meandering current  
 178 that together with the Atlantic-Ionian Stream (AIS), transports Atlantic Water from the western to the eastern Mediterranean  
 179 Sea (Poulain et al., 2012, 2013; Menna et al., 2019a; Figure 1(a)). Although the NWM, SWM and ION sectors have different  
 180 oceanographic characteristics, they showed a similar response to the 2022 MHW (Figure 2(a-c)). Most  $\bar{T}_a$  profiles belong to  
 181 Category 1 and the mean MHW depth falls into the 20-25 m layer (Table 2). Profiles, characterized by shallow MHW

182 penetration (blue lines in Figures 2(a-c)), showed decreasing warming in the first 50 m with the maximum  $\tilde{T}_a$  close to the  
183 surface (22.2-22.5 m; Table 2). The layer between 50 and 100 m depth showed a negative  $\tilde{T}_a$  with maxima of  $-0.65^\circ\text{C}$ ,  $-0.2^\circ\text{C}$   
184 and  $-0.53^\circ\text{C}$  at 50 m, 70 m and 40 m depth, in the NWM, SWM and ION sectors, respectively (Figures 2(a-c)). The median  
185 profiles derived from the FLOAT climatology (black lines in Figure 2(a-c)) do not exhibit this negative anomaly (or only to  
186 a very small extent), suggesting, therefore, a possible link between this behavior and the occurrence of the 2022 MHW. Below  
187 100 m depth, the  $\tilde{T}_a$  becomes positive again with mean values of  $\sim 0.3^\circ\text{C}$  in the intermediate layer and values lower than  $0.12^\circ\text{C}$   
188 in the deep layer. Profiles characterized by intermediate MHW penetration (red lines in Figures 2(a-c); MHW depth between  
189 570 m and 650 m, Table 2) were located in coastal areas of the Western Mediterranean and in frontal zones in the ION sector,  
190 and showed positive  $\tilde{T}_a$  throughout the water column, with values in the range of  $0.3 - 0.6^\circ\text{C}$ . Profiles, characterized by deep  
191 MHW penetration (green lines in Figures 2(a-c); MHW depth  $\sim 1400$  m, Table 2), showed the largest  $\tilde{T}_a$  in the surface layer  
192 in the two sectors of the West Mediterranean ( $> 0.8^\circ\text{C}$ ), while the ION sector depicted the largest anomalies in the intermediate  
193 layer ( $> 0.5^\circ\text{C}$ ). These results are consistent with the warming trend of the Western Mediterranean Sea over the last 15 years  
194 of  $0.09 \pm 0.02$  ( $0.03 \pm 0.01$ )  $^\circ\text{C}\cdot\text{yr}^{-1}$  for surface (intermediate) waters (Kubin et al., 2023).

195 The PG is located on the eastern side of the northern Ionian Sea, southwest of the Peloponnese coast (Figure 1(a)). It is a sub-  
196 basin anticyclonic feature (diameter of  $\sim 120$  km; Pinardi et al., 2015) which extends from the surface down to 800-1000 m  
197 depth (Malanotte-Rizzoli et al., 1997; Kovacevic et al., 2015) and it is forced by the Etesian winds (Ayoub et al., 1998;  
198 Mkhinini et al., 2014; Menna et al., 2021). In the late summer/fall the Etesian winds amplify their acceleration and the wind  
199 shear in the region of the western Cretan straits (Mkhinini et al., 2014) therefore, larger anticyclonic vorticities are observed  
200 during these months of the PG region (Menna et al., 2019a). In the sector PG,  $\tilde{T}_a$  profiles for the three categories showed  
201 positive temperature anomalies in the first 800 m of the water column which coincides with the vertical extension of the gyre  
202 itself (Figure 2(d)). Profiles that fall into Category 1 showed decreasing warming in the first 70 m, anomaly values close to  
203 zero in the 70-150 m layer and increasing warming in the 150-400 m layer. The mean anomaly in the intermediate layer of  
204 Category 1 is  $0.3^\circ\text{C}$  (Table 2). Category 2 profiles were retrieved mainly in the coastal area near the Peloponnese while  
205 Category 3 profiles were found within the gyre area. Categories 2 and 3 showed strong warming in the surface layer ( $0.97^\circ\text{C}$   
206 and  $1.14^\circ\text{C}$ , respectively), a mean warming in the range of  $0.3-0.6^\circ\text{C}$  in the intermediate layer and no warming compared to  
207 the SDC climatology was observed in the deep layer (Table 2).

208 The SAP is one of the sites of open ocean convection in the Mediterranean Sea, characterized by a complex thermohaline  
209 circulation that influences the physical and biogeochemical properties of the dense waters formed in its interior and the strength  
210 of winter convection (Di Biagio et al., 2023; Menna et al., 2022 OSR6; Pirro et al., 2022). This sector showed positive  
211 temperature anomalies in all layers and in all categories (Figure 2(d)). Most profiles belong to Category 3 with a mean MHW  
212 depth of  $\sim 950$  m and maximum  $\tilde{T}_a$  at  $\sim 80$  m depth. The largest mean warming was observed in the surface layer of each  
213 category ( $0.6-1.04^\circ\text{C}$ ) followed by the deep layer, which had an exceptional warming of  $\sim 0.6^\circ\text{C}$ , and finally by the  
214 intermediate layer, with a mean warming of  $\sim 0.4^\circ\text{C}$  (Table 2).

215 All five sectors showed a larger warming than the FLOAT climatology with a mean temperature increase in spring-summer  
216 2022 between  $0.2^{\circ}\text{C}$  and  $0.8^{\circ}\text{C}$  in response to the MHW event (Table 2). Some differences in warming observed among the  
217 sectors are related to their peculiar hydrological and dynamical characteristics. During the spring-summer period, the surface  
218 layer of the NWM and SWM sectors and partially of the ION sector, was characterized by both larger stratifications and  
219 stratification anomalies compared to the FLOAT climatology (Figures 3(a), 3(b)). Strong stratification prevents vertical heat  
220 penetration causing negative  $\tilde{T}_a$  in the 50-100 m layer (Figure 2(a-c)). In the PG sector, summer-spring stratification anomaly  
221 was consistent with climatology (Figure 3(b)), and vertical heat penetration was closely related to the gyre dynamics. In the  
222 SAP sector, stratification during the summer-spring period was lower than climatology suggesting an instability of the water  
223 column and therefore the transport of the vertical heat to the deep layers. The median of all profiles available in spring-summer  
224 2022, when not categorized, closely aligns with the median of profiles in category C1 (Figures 3(c), 3(d)). This condition arises  
225 because category C1 consistently boasts the highest number of profiles across various sectors.



227 **Figure3: (a) Monthly averaged Brunt - Väisälä frequency squared (N<sup>2</sup>) computed in the surface layer (0-150 m) using 2022 Argo**  
228 **float data. (b) Monthly averaged Brunt Brunt—Väisälä frequency squared anomaly (N<sup>2</sup> anomaly) computed in the surface layer**  
229 **with respect to the FLOAT climatology. (c) Median Temperature anomaly (°C) computed in the warm season (May - September)**  
230 **from Argo floats profiles in 2022 and (d) in 2001-2018 with respect to the SDC climatology. (e) Median Temperature anomaly (°C)**  
231 **computed in fall period (October - December) from Argo floats profiles in 2022 and (e) in 2001-2018 with respect to the SDC**  
232 **climatology). (g) Daily Sea Surface Temperature (°C) in the ION sector (black box) for late November and (h) early December**  
233 **2022.**

234 Larger warming of the water column was observed in fall 2022 compared to the SDC climatology in all sectors, except for the  
235 surface layer of the ION and PG sectors (Figure 3e). The stronger spring-summer stratification observed in the NWM and  
236 SWM sectors (Figures 3(a), 3(b)) corresponds to enhanced vertical heat propagation in the surface and intermediate layers in  
237 fall 2022 (Figure 3(e), Table 2). Negative  $\tilde{T}_a$  values in the surface layer of the ION sector were attributed to an upwelling event  
238 along the southern coast of Sicily between November and December 2022 as shown by the Sea Surface Temperature (Product  
239 ref. no. 2, Table 1; (Figures 3(g), 3(h)). The northern part of the Sicily Channel is an area of strong eddy kinetic energy (Poulain  
240 et al., 2012) influenced by Ekman transport and advection of waters from the western to the eastern Mediterranean (Molcard  
241 et al., 2002; Falcini et al., 2015; Schroeder et al., 2017; Menna et al., 2019b). The cold waters upwelled off the southern coast  
242 of Sicily in November 2022 (Figure 3(g)) were advected to the Ionian Sea through the Atlantic-Ionian Stream and the Mid-  
243 Ionian Jet pathways (Figure 1(a)), and gradually cooling the waters in the ION sector (Figure 3(h)). The negative anomaly in  
244 the surface layer of the ION sector is not limited only to 2022 but is a permanent characteristic of the area related to the  
245 upwelling phenomena, as confirmed by the  $\tilde{T}_a$  profile derived from the FLOAT climatology (orange line in Figure 3(f)) and  
246 by trends of the OHC anomaly estimated by Dayan et al. (2023) over the period 1987-2019. Negative  $\tilde{T}_a$  values in the PG  
247 sector were imputable to the typical downwelling process of this region associated with the gyre dynamics. The downwelling  
248 contributed to the vertical propagation of the 2022 MHW, with a strong spring-summer warming in the first 800 m of the water  
249 column (Figure 2d), keeping the stratification values similar to the FLOAT climatology (no significant increases of N<sup>2</sup> anomaly  
250 was registered due to the 2022 heatwave; Figure 3(b)). In this way, fall cooling can penetrate deep into the water column  
251 causing, therefore, negative  $\tilde{T}_a$  values in the surface layer (Figure 3(e).; Table 2).

252 In recent years, the SAP is experiencing a significant temperature increase in the deep layer (trend of  $\sim 0.06^\circ \text{C}\cdot\text{yr}^{-1}$  in the  
253 2013-2020 period according to Kubin et al., 2023) and salinity in the surface and intermediate layers (Mihanovich et al., 2021;  
254 Menna et al., 2022 OSR6) with potential future effects on the whole thermohaline cell of the Eastern Mediterranean. It is of  
255 general understanding that convection sites contribute to the propagation of the MHWs signal from the surface to the  
256 subsurface interior of the water column (Dayan et al., 2023; Kubin et al., 2023) but specific analysis at the local scale are not  
257 yet available (Juza et al., 2022). Our results show a fair significant warming of the SAP in both spring summer (Figures 2(e)  
258 and 3(c)) and fall (light blue line in Figure 3(f)) 2022 and a significant positive anomaly of FLOAT climatology compared to  
259 SDC one (black line in Figure 2(e) and light blue line in Figure 3(f)). In fall, largest  $\tilde{T}_a$  in the SAP were observed in the deep

260 layer ( $\sim 0.69$  °C); Table 2, Figure 3(e)). Mean profiles derived from Float Climatology (black line in Figure 2(e) and light  
261 blue line in Figure 3(f)) showed positive values compared to SDC one, confirming the warming trend throughout the water  
262 column over the past decade. Beyond the impact of the global warming of the Mediterranean Sea, the 2022 MHW leads to an  
263 additional heating in the SAP, which is transferred to the deeper layers favored by dynamical features of this area.

264 **This study aims to characterize the 2022 MHW in the subsurface layers, and attempts to explain the mechanisms that drive the**  
265 **heat penetration to deep layers. However, further and more detailed investigations are needed to better support this last**  
266 **conclusion.** We show that the effects of the 2022 MHW are felt in all layers of the Mediterranean Sea with vertical heat  
267 propagation extending from the surface to  $\sim 1500$  m depth. In the surface layer, heat penetration and storage are related to the  
268 strength of the stratification and/or advection from adjacent regions. In contrast, the transport and the storage of heat in the  
269 intermediate and deep layers are closely linked to the dynamics of each area. These considerations are in line with the findings  
270 of Elzahaby et al. (2021) and Zhang et al. (2023), who noted that shallower MHWs are primarily influenced by surface air-sea  
271 fluxes, whereas deeper MHWs are predominantly driven by advection, manifesting distinct dynamics across various oceanic  
272 regions.

273 In the western Mediterranean and western Ionian Sea sectors, heat is mainly stored in the surface layer (shallow MHW depths  
274 and stronger stratification) so that this layer is significantly warmer than the climatology even during the following fall.  
275 Although deep MHW penetration in these regions is limited to coastal and frontal/eddies zones, it reaches the higher MHW  
276 depth estimated during the event. Sectors characterized by specific dynamics conditions (downwelling, convection) quickly  
277 distribute the heat in the water column even during the event. **Intermediate layers exhibit comparable heating both during and**  
278 **after the MHW event, implying that heat can be stored there for extended periods and can be regarded as a long-term signal.**

279 The warming signal in the intermediate and deep layers could also be influenced by heat advection from adjacent basins  
280 however, we are aware that this topic needs to be studied in more detail in the future. In this context, the use of two  
281 climatologies and the cumulative anomaly threshold in the present analysis should have eliminated most of the signal  
282 associated with the ocean warming trend and advection therefore, the additional warming registered in spring-summer 2022  
283 compared to the FLOAT climatology can be attributed to the effects of the 2022 MHW along the entire water column. Further  
284 studies are needed to investigate the effects that this warming may have on the physical and biological oceanic processes with  
285 implications on the thermohaline circulation of the entire Mediterranean Sea.

286

287

288 Competing interests. The contact author has declared that neither they nor their co-authors have any competing interests.

289

290 Author contributions. Conceptualization of the study was done by AP, MM and RM. AP and MM prepared the original  
291 manuscript. AP, MM, RM, EM, AG, GN, EK and MJ reviewed and edited the manuscript. AP, MM and RM created the  
292 methodology. AP, MM, RM and EK created the codes and performed the formal analysis. AP, MM, RM conducted the  
293 investigation. AG, AB and MP curated the data. EM was in charge of Argo-Italy infrastructure management and funding  
294 acquisition. All authors have read and agreed to the published version of the paper.

## 295 **References**

296 Argo: Argo float data and metadata from Global Data Assembly Centre (Argo GDAC). SEANOE.  
297 <https://doi.org/10.17882/42182>, 2023.

298 Ayoub, N., Le Traon, P.-Y., and De Mey, P.: A description of the Mediterranean surface variable circulation from combined  
299 ERS-1 and TOPEX/POSEIDON altimetric data. *J.Mar. Syst.* 18, 3–40, [https://doi.org/10.1016/S0924-7963\(98\)80004-3](https://doi.org/10.1016/S0924-7963(98)80004-3), 1998.

300 Bensoussan, N., Chiggiato, J., Buongiorno Nardelli, B., Pisano, A. and Garrabou, J.: Insights on 2017 marine heat waves in  
301 the Mediterranean sea. *J. Oper. Ocean.*, 12 (1), s26–s30, <https://doi.org/10.1080/1755876X.2019.163307>, 2019.

302 Darmaraki, S., Somot, S., Sevault, F. and Nabat, P.: Past variability of Mediterranean Sea marine heatwaves, *Geophys. Res.*  
303 *Lett.*, 46 (16), 9813–9823, <https://doi.org/10.1029/2019GL082933>, 2019.

304 Dayan, H., McAdam, R., Juza, M., Masina, S. and Speich, S.: Marine heat waves in the Mediterranean Sea: An assessment  
305 from the surface to the subsurface to meet national needs. *Front. Mar. Sci.*, <https://doi.org/10.1045138>,  
306 1010.3389/fmars.2023.1045138, 2023.

307 Di Biagio, V., Martellucci, R., Menna, M., Teruzzi, A., Amadio, C., Mauri, E., & Cossarini, G.: Dissolved oxygen as an  
308 indicator of multiple drivers of the marine ecosystem: the southern Adriatic Sea case study. *State of the Planet*, 1, 1-13,  
309 <https://doi.org/10.5194/sp-1-osr7-10-2023>, 2023.

310 Elzahaby, Y. and Schaffer, A.: Observational insight into the subsurface anomalies of marine heatwaves. *Front. Mar. Sci.*,  
311 6:745, <https://doi.org/10.3389/fmars.2019.00745>, 2019.

312 Elzahaby, Y., Schaeffer, A., Roughan, M., & Delaux, S.: Oceanic circulation drives the deepest and longest marine heatwaves  
313 in the East Australian Current system. *Geoph. Res. Lett.*, 48(17), <https://doi.org/10.1029/2021GL094785>, 2021.

314 Escudier, R., Clementi, E., Cipollone, A., Pistoia, J., Drudi, M., Grandi, A., Lyubartsev, V., Lecci, R., Aydogdu, A., Delrosso,  
315 D., Omar, M., Masina, S., Coppini, G. and Pinardi, N.: A High Resolution Reanalysis for the Mediterranean Sea. *Front. Earth*  
316 *Sci.*, 9:702285, <https://doi.org/10.3389/feart.2021.702285>, 2021.

317 Falcini, F. and Salusti, E.: Friction and mixing effects on potential vorticity for bottom current crossing a marine strait: an  
318 application to the Sicily Channel (central Mediterranean Sea). *Ocean Sci.*, 11, 391–403, [https://doi.org/10.5194/os-11-391-](https://doi.org/10.5194/os-11-391-2015)  
319 2015, 2015.

320 Galli, G., Solidoro C., and Lovato T.: Marine heat waves hazard 3D maps and the risk for low motility organisms in a warming  
321 Mediterranean Sea. *Front. Mar. Sci.*, 4: 136, <https://doi.org/10.3389/fmars.2017.00136>, 2017.



- 322 Garrabou, J. et al.: Marine heatwaves drive recurrent mass mortalities in the Mediterranean Sea. *Global Change Biology*,  
323 <https://doi.org/10.1111/gcb.16301>, 2022
- 324 Hobday, A. J., Alexander, L. V., Perkins, S. E., Smale, D. A., Straub, S. C., Oliver, E. C., Benthuisen, J. A., Burrows, M. T.,  
325 Donat, G. M., Feng, M., Holbrook, N. J., Moore, P. J., Scannell, H. A., Gupta, A. S. and Wernberg T.: A hierarchical approach  
326 to defining marine heatwaves. *Prog. Oceanogr.* 141, 227–238, <https://doi.org/10.1016/j.pocean.2015.12.014>, 2016.
- 327 Holbrook, N. J., Gupta, A. S., Oliver, E. C., Hobday, A. J., Benthuisen, J. A., Scannell, H. A., et al.: Keeping pace with marine  
328 heatwaves. *Nat. Rev. Earth Env.*, 1 (9), 482– 493, <https://doi.org/10.1038/s43017-020-0068-4>, 2020.
- 329 Ibrahim, O., Mohamed, B., and Nagy, H.: Spatial variability and trends of marine heat waves in the Eastern Mediterranean  
330 Sea over 39 years. *J. Mar. Sci. Eng.*, 9 (6), 643, <https://doi.org/10.3390/jmse9060643>, 2021.
- 331 Intergovernmental Panel on Climate Change (IPCC): Summary for Policymakers. In: *Climate Change 2023, Synthesis Report*,  
332 *Summary for Policymakers, Core Writing Team, Lee, H. and Romero, J.*, 36,  
333 [https://www.ipcc.ch/report/ar6/syr/downloads/report/IPCC\\_AR6\\_SYR\\_SPM.pdf](https://www.ipcc.ch/report/ar6/syr/downloads/report/IPCC_AR6_SYR_SPM.pdf), 2023.
- 334 Juzá, M., Fernández-Mora, A., and Tintoré, J.: Sub-Regional marine heat waves in the Mediterranean Sea from observations:  
335 long-term surface changes, subsurface and coastal responses. *Front. Mar. Sci.* 9, 785771, <https://doi.org/10.3389/fmars.2022.785771>, 2022.
- 337 Kovačević, V., Ursella, L., Gačić, M., Notarstefano, G., Menna, M., Bensi, M., and Poulain, P.-M.: On the Ionian thermohaline  
338 properties and circulation in 2010–2013 as measured by Argo floats. *Acta Adriat.*, 56(1): 97 - 114, 2015.
- 339 Kubin, E., Menna, M., Mauri, E., Notarstefano, G., Mieruch, S., and Poulain, P.-M.: Heat content and temperature trends in  
340 the Mediterranean Sea as derived from Argo float data. *Front. Mar. Sci.* 10, 1271638,  
341 <https://doi.org/10.3389/fmars.2023.1271638>, 2023.
- 342 Liqueste, C., Piroddi, C., Macias, D., Druon, J. N., and Zulian, G.: Ecosystem services sustainability in the Mediterranean Sea:  
343 assessment of status and trends using multiple modelling approaches. *Sci. Rep.* 6 (1), 1–14, <https://doi.org/10.1038/srep34162>,  
344 2016.
- 345 Malanotte-Rizzoli, P., Manca, B. B., Ribera D’Alcalà, M., Theocharis, A., Bergamasco, A., Bregant, D., Budillon, G.,  
346 Civitarese, G., Georgopoulos, D., Michelato A., Sansone, E., Scarazzato, P., Souvermezoglou, E.: A synthesis of  
347 the Ionian Sea hydrography, circulation and water masses pathways during POEM-Phase I. *Progr. Oceanogr.*, 39, 153–204,  
348 [https://doi.org/10.1016/S0079-6611\(97\)00013-X](https://doi.org/10.1016/S0079-6611(97)00013-X), 1997.
- 349 Martín-Lopez, B., Oteros-Rozas, E., Cohen-Shacham, E., Santos-Martín, F., Nieto-Romero, M., Carvalho-Santos, C., et al.:  
350 Ecosystem services supplied by mediterranean basin ecosystems, in *Routledge handbook of ecosystem services*. Eds. M.  
351 Potschin, R. Haines-Young, R. Fish and R. K. Turner (London: Routledge), 405–414, 2016.
- 352 Martínez, J., Leonelli, F. E., García-Ladona, E., Garrabou, J., Kersting, D., Bensoussan, N., & Pisano, A.: Evolution of marine  
353 heatwaves in warming seas: the Mediterranean Sea case study. *Front. Mar. Sci.*, <https://doi.org/10.3389/fmars.2023.1193164>,  
354 2023.
- 355 Marullo, S., Serva, F., Iacono, R., Napolitano, E., di Sarra, A., Meloni, D., ... & Santoleri, R.: Record-breaking persistence of  
356 the 2022/23 marine heatwave in the Mediterranean Sea. *Env. Res. Lett.*, 18(11), 114041, <https://doi.org/10.1088/1748-9326/ad02ae>, 2023.

- 358 Menna, M., Suarez, N. R., Civitarese, G., Gačić, M., Rubino, A., and Poulain, P. M.; Decadal variations of circulation in the  
359 Central Mediterranean and its interactions with mesoscale gyres. *Deep Sea Res. II*, 164, 14-24,  
360 <https://doi.org/10.1016/j.dsr2.2019.02.004>, 2019a.
- 361 Menna, M., Poulain, P. M., Ciani, D., Doglioli, A., Notarstefano, G., Gerin, R., Rio, M. H. Santoleri, R., Gauci, A. and Drago,  
362 A.: New Insights of the Sicily Channel and Southern Tyrrhenian Sea Variability. *Water*, 11, 1355,  
363 <https://doi.org/10.3390/w11071355>, 2019b.
- 364 Menna, M., Gerin, R., Notarstefano, G., Mauri, E., Bussani, A., Pacciaroni, M., and Poulain, P. M.: On the circulation and  
365 thermohaline properties of the Eastern Mediterranean Sea. *Fron. Mar. Sci.*, 8, 671469,  
366 <https://doi.org/10.3389/fmars.2021.6714692>, 2021.
- 367 Menna, M., Martellucci, R., Notarstefano, G., Mauri, E., Gerin, R., Pacciaroni, M., Bussani, A., Pirro, A., Poulain, P. M.:  
368 Record-breaking high salinity in the South Adriatic Pit in 2020. *J. Oper. Oceanogr.*, s199-s205,  
369 <https://doi.org/10.1080/1755876X.2022.2095169>, 2022.
- 370 Mihanović, H., Vilibić, I., Šepić, J., Matić, F., Ljubešić, Z., Mauri, E., Gerin, R.: Observation, preconditioning and recurrence  
371 of exceptionally high salinities in the Adriatic Sea. *Front. Mar. Sci.*, 8:834. <https://doi.org/10.3389/fmars.2021.672210>, 2021.
- 372 Mills, K. E., Pershing, A. J., Brown, C. J., Chen, Y., Chiang, F. S., Holland, D. S., et al.: Fisheries management in a changing  
373 climate: lessons from the 2012 ocean heat wave in the Northwest Atlantic. *Oceanography* 26 (2), 191–195,  
374 <https://doi.org/10.5670/oceanog.2013.27>, 2013.
- 375 Molcard, A., Gervasio, L., Gria, A., Gasparini, G. P., Mortier, L., Ozgokmen, T. M.: Numerical investigation of the Sicily  
376 Channel dynamics: density currents and water mass advection. *J. Mar. Syst.*, 36, 219–238, [https://doi.org/10.1016/S0924-7963\(02\)00188-4](https://doi.org/10.1016/S0924-7963(02)00188-4), 2002.
- 378 Mkhinini, N., Coimbra, A. L. S., Stegner, A., Arsouze, T., Taupier-Letage, I., and Beranger, K.: Long-lived mesoscale eddies  
379 in the Eastern Mediterranean Sea: analysis of 20 years of AVISO geostrophic velocities. *J. Geophys. Res. Oceans* 119, 8603–  
380 8626, <https://doi.org/10.1002/2014JC010176>, 2014.
- 381 Oliver, E. C., Donat, M. G., Burrows, M. T., Moore, P. J., Smale, D. A., Alexander, L. V., Benthuisen, J. A., Feng, M., Gupta,  
382 A. S., Hobday, A. J., Holbrook, N. J., Perkins-Kirkpatrick, S. E., Scannell, H. E., Straub, S. C. and Wernberg, T.: Longer and  
383 more frequent marine heatwaves over the past century. *Nat. Commun.*, 9:1324, <https://doi.org/10.1038/s41467-018-03732-9>,  
384 2018.
- 385 Pinardi, N., Zavatarelli, M., Adani, M., Coppini, G., Fratianni, C., Oddo, P., Simoncelli, S., Tonani, M., Lyubartsev, V.:  
386 Mediterranean Sea large-scale low-frequency ocean variability and water mass formation rates from 1987 to 2007: a  
387 retrospective analysis. *Prog. Oceanogr.* 132, 318–332, <https://doi.org/10.1016/j.pocean.2013.11.003>, 2015.
- 388 Pastor, F., & Khodayar, S.: Marine heat waves: Characterizing a major climate impact in the Mediterranean. *Science of The*  
389 *Total Env.*, 861, 160621, <https://doi.org/10.1016/j.scitotenv.2022.160621>, 2023.
- 390 Pirro, A., Mauri, E., Gerin, R., Martellucci, R., Zuppelli, P. and Poulain, P. M.: New insights on the formation and breaking  
391 mechanism of convective cyclonic cones in the South Adriatic Pit during winter 2018. *J. Phys. Oceanogr.*, 52(9), 2049-2068,  
392 <https://doi.org/10.1175/JPO-D-21-0108.1>, 2022.
- 393 Poulain, P. M., Menna, M., and Mauri, E.: Surface geostrophic circulation of the Mediterranean Sea derived from drifter and  
394 satellite altimeter data. *J. Phys. Oceanogr.*, 42(6), 973-990, <https://doi.org/10.1175/JPO-D-11-0159.1>, 2012.

- 395 Poulain, P. M., Bussani, A., Gerin, R., Jungwirth, R., Mauri, E., Menna, M. and Notarstefano, G.: Mediterranean surface  
396 currents measured with drifters: From basin to subinertial scales. *Oceanography* 26 (1), 38–47,  
397 <https://doi.org/10.5670/oceanog.2013.03>, 2013.
- 398 Poulain, P. M., Centurioni, L., Özgökmen, T., Tarry, D., Pascual, A., Ruiz, S., Mauri, E., Menna, M. and Notarstefano, G.: On  
399 the structure and kinematics of an Algerian Eddy in the southwestern Mediterranean Sea. *Rem. Sens.*, 13(15), 3039,  
400 <https://doi.org/10.3390/rs13153039>, 2021.
- 401 Pastor, F. and Khodayar, S.: Marine heat waves: Characterizing a major climate impact in the Mediterranean. *Sci. Tot. Env.*,  
402 861, 160621, <https://doi.org/10.1016/j.scitotenv.2022.160621>, 2022.
- 403 Santora, J. A., Mantua, N. J., Schroeder, I. D., Field, J. C., Hazen, E. L., Bograd, S. J., et al.: Habitat compression and ecosystem  
404 shifts as potential links between marine heatwave and record whale entanglements. *Nat. Commun.* 11 (1), 1–12,  
405 <https://doi.org/10.1038/s41467-019-14215-w>, 2020.
- 406 Scannell, H. A., Johnson, G. C., Thompson, L., Lyman, J. M., and Riser, S. C.: Subsurface evolution and persistence of marine  
407 heatwaves in the Northeast Pacific. *Geophys. Res. Lett.*, 47, e2020GL090548, <https://doi.org/10.1029/2020GL090548>, 2020.
- 408
- 409 Schaeffer, A., and Roughan, M.: Subsurface intensification of marine heatwaves off southeastern Australia: the role of  
410 stratification and local winds. *Geoph. Res. Lett.*, 44 (10), 5025–5033, <https://doi.org/10.1002/2017gl073714>, 2017.
- 411 Schroeder, K., Chiggiato, J., Josey, S.A., Borghini, M., Aracri, S., Sparnocchia, S.: Rapid response to climate change in a  
412 marginal sea. *Sci. Rep.*, 7, 4065, <https://doi.org/10.1038/s41598-017-04455-5>, 2017.
- 413 Shijian H., S., Li, S., Zhang, Y., Guan, C., Du, Y., Feng, M., Anodo, K., Wang, F., Schiller, A. and Hu, D.: Observed strong  
414 subsurface marine heatwaves in the tropical western Pacific Ocean. *Env. Res. Lett.*, 16(10), 104024, <https://doi.org/10.1088/1748-9326/ac26f2>, 2021.
- 415
- 416 Simon, A., Pires, C., Frölicher, T. L., & Russo, A.: Long-term warming and interannual variability contributions' to marine  
417 heatwaves in the Mediterranean. *Weather and Climate Extremes*, 42, 100619, <https://doi.org/10.1016/j.wace.2023.100619>,  
418 2023.
- 419 Smale, D. A., Wernberg, T., Oliver, E. C., Thomsen, M., Harvey, B. P., Straub, S. C., et al.: Marine heatwaves threaten global  
420 biodiversity and the provision of ecosystem services. *Nat. Climate Change*, 9 (4), 306–312, [https://doi.org/10.1038/s41558-](https://doi.org/10.1038/s41558-019-0412-1)  
421 [019-0412-1](https://doi.org/10.1038/s41558-019-0412-1), 2019.
- 422 Von Schuckmann, K., Palmer, M. D., Trenberth, K. E., Cazenave, A., Chambers, D., Champollion, N., Hansen, J., Josey, S.  
423 A., Loeb, N., Mathieu, P. P., Meyssignac, B. and Wild, M.: An imperative to monitor earth's energy imbalance. *Nat. Clim.*  
424 *Change*, 6 (2), 138–144, [doi:10.1038/nclimate2876](https://doi.org/10.1038/nclimate2876), 2016.
- 425 Wernberg, T., Smale, D. A., Tuya, F., Thomsen, M. S., Langlois, T. J., De Bettignies, T., Bennet, S. and Rousseaux, C. S.: An  
426 extreme climatic event alters marine ecosystem structure in a global biodiversity hotspot. *Nat. Clim. Change*, 3, 78–82,  
427 <https://doi.org/10.1038/nclimate1627>, 2013.
- 428 Wong, A. P., Wijffels, S. E., Riser, S. C., Pouliquen, S., Hosoda, S., Roemmich, D., et al.: Argo Data 1999–2019: Two Million  
429 Temperature-Salinity Profiles and Subsurface Velocity Observations From a Global Array of Profiling Floats. *Front. Mar. Sci.*,  
430 7(700), <https://doi.org/10.3389/fmars.2020.00700>, 2020.

431 Zhang, Y., Du, Y., Feng, M., & Hobday, A. J.: Vertical structures of marine heatwaves. *Nature Communications*, 14(1), 6483,  
432 <https://doi.org/10.1038/s41467-023-42219-0>, 2023.

433

#### 434 **References for Table 1**

435 Product ref no.1

436 EU Copernicus Marine Service Product: Mediterranean Sea- In-Situ Near Real Time Observations, Mercator Ocean  
437 International [data set], <https://doi.org/10.48670/moi-00044>, 2022.

438 H. Wehde, K. V. Schuckmann, S. Pouliquen, A. Grouazel, T Bartolome, J Tintore, M. De Alfonso Alonso-Munoyerro, T.  
439 Carval, V. Racapé and the INSTAC team: EU Copernicus Marine Service Quality Information Document for Mediterranean  
440 Sea- In-Situ Near Real Time Observations, INSITU\_MED\_PHYBGCWAV\_DISCRETE\_MYNRT\_013\_035, Issue 2.2,  
441 Mercator Ocean International, [https://catalogue.marine.copernicus.eu/documents/QUID/CMEMS-INS-QUID-013-030-  
442 036.pdf](https://catalogue.marine.copernicus.eu/documents/QUID/CMEMS-INS-QUID-013-030-036.pdf), last access: 19 May 2023, 2022.

443 In Situ TAC partners: EU Copernicus Marine Service Product User Manual for Mediterranean Sea- In-Situ Near Real Time  
444 Observations, INSITU\_MED\_PHYBGCWAV\_DISCRETE\_MYNRT\_013\_035, Issue 1.14, Mercator Ocean International,  
445 <https://catalogue.marine.copernicus.eu/documents/PUM/CMEMS-INS-PUM-013-030-036.pdf>, last access: 19 May 2023,  
446 2022.

447 Product ref no.2

448 EU Copernicus Marine Service Product: Mediterranean Sea Physics Reanalysis, Mercator Ocean International [data set],  
449 [https://doi.org/10.25423/CMCC/MEDSEA\\_MULTIYEAR\\_PHY\\_006\\_004\\_E3R11](https://doi.org/10.25423/CMCC/MEDSEA_MULTIYEAR_PHY_006_004_E3R11), 2022.

450 R. Escudier, E. Clementi, T. Nigam, A. Aydogdu, E. Fini, J. Pistoia, A. Grandi, P. Miraglio: EU Copernicus Marine Service  
451 Quality Information Document for Mediterranean Sea Physics Reanalysis, MEDSEA\_MULTIYEAR\_PHY\_006\_004, Issue  
452 2.3, Mercator Ocean International, [https://catalogue.marine.copernicus.eu/documents/QUID/CMEMS-MED-QUID-006-  
453 004.pdf](https://catalogue.marine.copernicus.eu/documents/QUID/CMEMS-MED-QUID-006-004.pdf), last access: 19 May 2023, 2022.

454 Rita Lecci, Massimiliano Drudi, Alessandro Grandi, Sergio Creti, Emanuela Clementi: EU Copernicus Marine Service Product  
455 User Manual for For Mediterranean Sea Physics Reanalysis, MEDSEA\_MULTIYEAR\_PHY\_006\_004, Issue 2.3, Mercator  
456 Ocean International, <https://catalogue.marine.copernicus.eu/documents/PUM/CMEMS-MED-PUM-006-004.pdf>, last access:  
457 19 May 2023, 2022.

458 Product ref no.3

459 EU Copernicus Marine Service Product: European Seas Gridded L 4 Sea Surface Heights And Derived Variables Nrt, Mercator  
460 Ocean International [data set], <https://doi.org/10.48670/moi-00142>, 2023.

461 M-I Pujol, G. Taburet and SL-TAC team.: EU Copernicus Marine Service Quality Information Document for European Seas  
462 Gridded L 4 Sea Surface Heights And Derived Variables Nrt,  
463 SEALEVEL\_EUR\_PHY\_L4\_NRT\_OBSERVATIONS\_008\_060, Issue 8.2, Mercator Ocean International,  
464 <https://catalogue.marine.copernicus.eu/documents/QUID/CMEMS-SL-QUID-008-032-068.pdf>, last access: 19 May 2023,  
465 2023.

466 M-I Pujol: EU Copernicus Marine Service Product User Manual for European Seas Gridded L 4 Sea Surface Heights And  
467 Derived Variables Nrt, SEALEVEL\_EUR\_PHY\_L4\_NRT\_OBSERVATIONS\_008\_060, Issue 7.0, Mercator Ocean  
468 International, <https://catalogue.marine.copernicus.eu/documents/PUM/CMEMS-SL-PUM-008-032-068.pdf>, last access: 19  
469 May 2023, 2022.

470 Product ref no.4

471 S. Simoncelli , P. Oliveri , G. Mattia. SeaDataCloud Mediterranean Sea - V2 Temperature and Salinity Climatology [dataset].  
472 <http://dx.doi.org/10.12770/3f8eaace-9f9b-4b1b-a7a4-9c55270e205a> [Accessed on 19 May 2023]

473 Simoncelli Simona, Oliveri Paolo, Mattia Gelsomina, Myroshnychenko Volodymyr, Barth Alexander, Troupin Charles (2020).  
474 SeaDataCloud Temperature and Salinity Climatology for the Mediterranean Sea (Version 2). Product Information Document  
475 (PIDoc). <https://doi.org/10.13155/77514>

476

477

478